DELPHI Collaboration DELPHI 97-07 PHYS 666
30 January, 1997

Energy and position reconstruction in the DELPHI Small Angle Tile Calorimeter

V. Obraztsov[1], **M. Paganoni**
CERN, European Organization for Nuclear Research, Geneva, Switzerland
S. Gumenyuk[1], **F. Terranova**
Dipartimento di Fisica, Università di Milano and INFN, Milan, Italy
M. Bigi, I. Gouz[1], **E. Migliore**
Dipartimento di Fisica, Università di Torino and INFN, Turin, Italy

1) On leave of absence from IHEP, Protvino, Russian Federation

Abstract

The STIC detector, installed in DELPHI in 1994, is a lead-scintillator calorimeter, segmented into towers projective to the interaction point. The light is collected by WLS fibers running perpendicularly to the sampling planes and read out by phototetrodes, which can operate inside the 1.2 T magnetic field of DELPHI. The main goal of the calorimeter is to measure the luminosity with an accuracy better than 0.1% which put high demands on the control of its geometry. The performance of the detector during the 1994-95 data taking is discussed in detail, with emphasis on the achieved energy and space resolution, the long-term stability and the efficiency of the detector.

1 Introduction.

At the beginning of 1994 the DELPHI collaboration installed a new electromagnetic calorimeter named STIC (Small angle TIle Calorimeter) [1], with the aims of providing a luminosity measurement with an accuracy of 0.1% at LEP I, and improving the hermeticity and energy resolution in the very-forward region for LEP II.

In fact the STIC project consists of 3 detectors:

- the calorimeter [2];
- the veto system [2].
- the silicon shower maximum detector [3];

This note reports mainly on the energy and position reconstruction in the STIC calorimeter, since they are key parameters for the luminosity measurement, that is based on the counting of the events of Bhabha scattering at small angles.

The precision of the mechanical structure, a good energy and position resolution and a uniform response are the most relevant features of the STIC in order to select, with high efficiency and well known acceptance, the Bhabha scattering events.

Up to now about four million Bhabha events were detected inside the STIC acceptance (2.4 million in 1994 and 1.6 million in 1995). The calorimeter was very stable and reliable and met all the requirements necessary for achieving and eventually exceeding the design accuracy in the luminosity measurement.

2 The STIC calorimeter.

The STIC calorimeter (see Fig.1) is made of two independent cylinders (called A and C) located at $\pm$ 2.2 m from the interaction point, covering the angular region 29 mrad $< \theta <$ 185 mrad w.r.t. the beams.

It consists of 47 layers, each made of a continous 3.0 mm thick lead plate (reinforced by 100 μm steel plates glued on each side for a total thickness of 3.4 mm) followed by 3 mm thick scintillator tiles, for a total depth of 27 X_0. The tiles are optically isolated from each other by 120 μm thick white Tyvek [1] and are mounted on the steel laminated lead planes by precision pins with a mechanical accuracy of 50 μm. This structure avoids non-uniformities and allows to define projective towers (10 rings and 16 sectors) with a precision better than 20 μm.

The light readout is done by WLS fibers running perpendicularly to the planes through holes drilled (punched) in the tiles (converter). The density of the fibers is about 0.8 fibers/cm^2 on average. This concept of light readout was invented a long time ago [4], and was recently revived by IHEP and INR groups from Russia[5].

In order to read out the light in the high magnetic field (1.2 T) of DELPHI, STIC uses Hamamatsu 1" R2149-03 tetrodes. Their behaviour has been studied in detail at the superconducting solenoid SOLEMI-1 (LASA laboratory, INFN-Milano[6]), showing an average gain of about 15, which is a factor two below the gain outside the magnetic field. For details of the calorimeter construction and components we refer to [7].

[1] Tyvek is Du Pont's registered trademark.

3 The energy reconstruction.

3.1 Common noise subtraction.

During 1994 and to a lesser extent in 1995 both sides of STIC were affected by a common mode noise due to electromagnetic disturbances caused mainly by the motors of the LEP collimators.

The calculation of the correlation coefficients for the common noise showed an almost full correlation for the 80 towers of a module. As the electromagnetic showers occupy, on average, 10-20 towers, we were able to measure for each module, on an event by event basis, the common noise to be subtracted from the static pedestals. This was done by fitting, in the distributions of the 80 ADCs, the position of the leftmost peak, corresponding to the towers without signals.

The distribution of the pedestal widths of all the counters is shown in Fig.2, before and after common noise subtraction. The effect of this correction is clearly visible in the shift of the distribution to smaller values, compatible with the intrinsic noise of the readout electronics. The average width of the pedestals is 1 count, which translates into 20 MeV. This procedure of common noise subtraction improves by 10% the energy resolution for 45 GeV showers and, what is more relevant for the luminosity measurement, it strongly reduces the non-gaussian tails in the distribution of the energy response to Bhabha events.

Furthermore a correlation in noise was also found between the two modules of each side, as shown in the scatter plots of Fig.3.

3.2 Clustering algorithm

In the clustering algorithm all the towers with a measured energy larger than 500 MeV are considered as seeds for a shower. The procedure starts from the most energetic seed and associates to it any nearby tower with an energy deposition larger than 5 % of the energy of the seed. The clustering is repeated for the remaining towers until all seeds are associated to a shower. In case of overlapping between two showers, the energy is shared on the basis of the energy depositions in the two central towers.

The distribution of the number of towers associated to the most energetic shower is shown in Fig. 4, while Fig. 5 gives the number of showers per event in a STIC arm.

3.3 Calibration

In order to achieve a good energy resolution, a precise knowledge of the calibration coefficients for all the STIC towers is needed. Even the variation with time of the STIC energy response, shown in Fig.6 for the sample of Bhabha events, have to be accounted for, by repeating the calibration procedure each month. This aging effect (2 % decrease per year) will not cause any significant degradation of the performance of the detector as long as it is regularly recalibrated. A possible explanation of the aging is the radiation damage of the scintillator and/or fibers due to the synchrotron radiation.

The non radiative Bhabha events, used for the calibration, were selected by tight energy and acollinearity cuts:

$$\begin{aligned} |R_C - R_A| &< 1 \text{ cm} \\ ||\phi_C - \phi_A| - 180^o| &< 8^o \end{aligned}$$

$$
\begin{aligned}
|E_A - E_{beam}| &< 0.15 E_{beam} \\
|E_C - E_{beam}| &< 0.15 E_{beam}
\end{aligned}
$$

where E_A (E_C), R_A (R_C), ϕ_A (ϕ_C) are the reconstructed energy, radius and azimuthal angle of the most energetic shower on the A (C) side. The calibration was performed on this sample in 3 to 5 iterations.

We calculated the energy of a shower according to a simple linear model:

$$
E_{meas} = \sum_{i=1}^{N_{chan}} c_i a_i, \tag{1}
$$

where $\{a_i\}$ are the raw amplitudes, after pedestal subtraction, and $\{c_i\}$ the calibration coefficients. The calibration coefficients were choosen in order to minimize the quantity F, where:

$$
F = \sum_{i_{ev}=1}^{N_{ev}} (E_{meas} - E_{beam})^2 \tag{2}
$$

This lead to a system of linear equations:

$$
\begin{aligned}
\sum_{j=1}^{N_{chan}} H_{ij} c_j &= B_i, \qquad \text{where} \\
H_{ij} &= \sum_{i_{ev}=1}^{N_{ev}} a_i^{i_{ev}} a_j^{i_{ev}}, \\
B_i &= \sum_{i_{ev}=1}^{N_{ev}} E_{beam} a_i^{i_{ev}},
\end{aligned} \tag{3}
$$

However, in the case of the STIC, the lateral energy leakage is significant in the inner and outer parts of the calorimeter, which means that the average deposited energy depends strongly on the position of the shower. To take this into account, we substituted in (3) the nominal E_{beam} with the "expected" energy E_{exp}, which was parametrized, as a function of the reconstructed radius of the shower, according to Monte Carlo.

Another modification of the algorithm took into account the instabilities in the numerical solution of (3), arising from the forward peaked radial distribution of the Bhabha events [2]. In order to make the distribution almost uniform each event was weighted, which caused the eigenvalues to acquire similar values [3].

The non uniform radial distribution of the Bhabha events has a second effect: a reasonable precision of the calibration coefficients can be achieved for the outer rings only by using a large data sample, while for the inner towers, even a small data sample contains enough statistics. Therefore the calibration procedure was modified in order to apply it only for part of the towers, while fixing the coefficients for the rest.

[2] It can be shown that the eigenvalues of the matrix H_{ij} are, to first approximation, proportional to the number of events hitting the corresponding towers and therefore the range of eigenvalues of the matrix can be very wide.

[3] Actually, the eigenvalues corresponding to the channels of the first ring of the calorimeter were 2-3 times less than others, because of the presence of the tungsten mask in this region. However the matrix H of the linear system (3) is far from being degenerate.

Taking into account all the modifications mentioned above, we arrived at the following set of equations:

$$\begin{aligned}
\sum_{j=1}^{N_{free}} H_{ij}c_j &= B_i \qquad (4)\\
H_{ij} &= \sum_{i_{ev}=1}^{N_{ev}} a_i^{i_{ev}} a_j^{i_{ev}} w_{i_{ev}}\\
B_i &= \sum_{i_{ev}=1}^{N_{ev}} (E_{exp}^{i_{ev}} - E_{fix}^{i_{ev}}) a_i^{i_{ev}} w_{i_{ev}}\\
w_{i_{ev}} &= \theta_{i_{ev}}^3\\
E_{fix}^{i_{ev}} &= \sum_{m=1}^{N_{fix}} c_m a_m^{i_{ev}}\\
E_{exp}^{i_{ev}} &= F(R^{i_{ev}})
\end{aligned}$$

where N_{free} is the number of towers to be calibrated, N_{fix} is the number of towers not involved in the calibration and E_{fix} is the energy deposited in these towers.

3.4 Correction for non-uniformities.

Due to the presence of the WLS fibers, the energy response of Shashlik-type calorimeters usually depends on the impact point of the incoming particle. The R-ϕ dependence of the STIC energy response to non-radiative Bhabha events is shown in Fig.7. Thanks to the homogeneous structure of the converter plates and to the high density of the WLS fibers, the non-uniformities are small, and can easily be corrected for, by mapping. The correction function E(R,ϕ) was calculated by averaging over the 8 ϕ-sectors of each STIC module.

The dependence of the energy resolution on the radial position is shown, before and after the correction for non-uniformity, in Fig.8. The resulting energy resolution for non-radiative Bhabha events was measured to be 2.7%.

3.5 Corrections with LEP running in bunch train mode.

During 1994 LEP made collisions with 8 bunches separated by 11 μsec, while during 1995 it ran with 4 trains of bunches, having from 2 to 4 "wagons", separated by 247 nsec [8]. The STIC trigger was modified to use a hit-patterns which was updated for each active wagon.

The strobe (track and hold) signal for the calorimeter ADC's was made by a coincidence of the wagon gate and the signals coming from the Veto system, which consists of 64 trapezoidal scintillator counters, assembled into 2 planes, put in front of the calorimeter. Because of this the STIC energy response was slightly influenced by the efficiency and the noise rate of the hodoscope.

In case of an inefficiency of the Veto, the strobe was given at the last wagon, which lead to strobing the falling edge of the calorimeter signal and consequently to a too small value of the measured energy for the events generated from previous wagons. This effect was present only in 411 events out of 1.6 million Bhabha events taken in 1995 (see Fig.9).

In case of noise in the Veto, present in 1.6% of the events in the Bhabha sample, the wagon tag was ambiguous and the strobe signal was provided by the first signal in the hodoscope, resulting again in a too small energy measurement if the event was generated from a later wagon. However, it turned out that, in most cases, it was possible to determine the true wagon number offline by comparing the hodoscope hitpatterns recorded for each wagon and the azimuthal position of the shower in the calorimeter. The measured energy distributions for various combinations of online and offline wagon tags are shown in Fig.10. Each distribution consists of a single peak in a well defined position, which makes an accurate correction possible.

3.6 Recontruction of the energy deposited in the dead channels.

During the first 25 days of 1994 data taking (i.e. the first 5 pb^{-1}) STIC had three channels not properly working. Two of them were located in the outer rings of the calorimeter and, due to the angular dependence of the Bhabha cross section, the number of lost events was found to be negligible for the luminosity measurement. The third channel instead was located in the fourth ring and therefore, in this case, a correction for the loss of events had to be applied. Various algorithms were developed in order to recover, on an event by event basis, the energy in the dead channel, on the basis of the pattern of energy deposition in the nearby channels.

The use of Artificial Neural Networks proved to be particularly effective [10].

The JETNET package was used to implement a Feed Forward Neural Network with back propagation updating [11]. The absolute precision in the reconstruction of the energy was estimated to be of the order of 110 MeV, which translated into an uncertainty in the measured luminosity smaller than 5 10^{-5}.

4 The position reconstruction.

Both the radius (R) and the azimuthal angle (ϕ) of the impact point of the shower can be measured on the basis of the sharing of the deposited energy between nearby calorimeter towers.

4.1 Reconstruction of the radius.

The precision of the radius reconstruction is a key point for the luminosity measurement, as it enters both in the definition of the geometrical acceptance and in the determination of the position of the interaction point [9].

The Bhabha events have unique features which are particularly well suited for achieving a good radial resolution:

- they all originate from the interaction point and therefore at each radius the angle at which the electrons hit the calorimeter is always the same;
- they have a peaked energy distribution.

Consequently, all the events at the same radial position have similar shower profiles. Furthermore, due to the projectivity of the STIC towers, the reconstructed radius is not sensitive to longitudinal fluctuations in the development of the shower.

The starting point for the measurement of the radial position of a shower consists in the reconstruction of its distance from the border between generic rings k and k+1. These distances were parametrized as a function of the estimator

$$\epsilon \;=\; \ln \frac{E_{in}}{E_{out}}$$

where E_{in} and E_{out} are defined as in Fig. 11.

The estimator was calculated by using data taken at a testbeam where the radial position of the impact point in the STIC was precisely measured by means of a silicon microstrip telescope (see Fig. 12).

In principle the radius of a shower can be calculated with respect to any ring border, for which $E_{in}, E_{out} > 0$:

$$R^k_{meas} = R^k + d^k(\epsilon)$$

However, we considered only the values R_{up} and R_{down}, which are measured with respect to the two ring borders delimiting the ring with the larger energy deposition. As measurement of R was taken its most probable value, calculated from R_{up}, R_{down} and their errors.

The resolution of the radial reconstruction, measured at the testbeam, was found to vary from 0.25 mm in a narrow region ($\pm$ 2 mm) around ring borders up to 1.2 mm in the central regions of the tower rings (see Fig. 13, 14).

The distribution of the reconstructed radius of the Bhabha events showed the overall $1/R^3$ dependence, as expected. The deviations which are visible in Fig.15 , could be explained by small biases, due to differences in the experimental conditions between the testbeam (where the $d^k(\epsilon)$ functions were measured) and LEP. [4]

For most physical applications these biases, which are of the order of the resolution, are negligible; however for delicate measurements, such as the determination of the position of the interaction point, we corrected for these effects, as explained in [9] and visible in Fig.16.

4.2 Reconstruction of the azimuthal angle.

The ϕ reconstruction algorithm is based on the energy sharing of the showers at the border between nearby ϕ-sectors. Similarly to the radius case, we used as an estimator

$$\epsilon = \ln \frac{E_{left}}{E_{right}} \tag{5}$$

where E_{left} and E_{right} are the energies deposited to the left and to the right of a border between two sectors (see Fig.17).

The dependence of the estimator on the distance to the sector border and the accuracy in the measurement of that distance were measured at the testbeam (see Fig.18) Due to the ring structure of the calorimeter the tower size in ϕ increases with R, which makes the resolution in ϕ worse in the outer rings.

[4] At the testbeam the electrons did not enter the calorimeter with an angle corresponding to the projective angle of the towers, as the calorimeter axis was tilted wrt the beam line by about 5 mrad.

5 Conclusions.

The STIC calorimeter has been operating at LEP since 1994 and satisfies the design requirements with a radial position resolution between 250 μm and 1.2 mm and an energy resolution of 2.7% for 45 GeV electrons.

Two year of operation at LEP have demonstrated that the detector can provide a reliable on-line luminosity measurement as well as a high precision offline estimate of the luminosity.

References

[1] The DELPHI Collaboration, "*Proposal for the replacement of the Small Angle Calorimeter of DELPHI*", CERN-LEPC/92-6

[2] S.J.Alvsvaag et al., IEEE Trans. Nucl. Sci. **42**(4)(1995)478.

[3] S.J.Alvsvaag et al., IEEE Trans. Nucl. Sci. **42**(4)(1995)469.
S.J. Alvsvaag et al., Nucl. Instr. and Meth. **A360**(1995)219

[4] H.Fessler et al., Nucl. Instr. and Meth. **A240**(1985)284.
B.Loher et al., Nucl. Instr. and Meth. **A254**(1987)26.

[5] G.Atojan et al., Nucl. Instr. Meth. **A320**(1992)144.

[6] M.Bonesini et al., Preprint INFN/AE-94/14, Milano, May, 1994.

[7] A. Benvenuti et al., Proceedings of *The International Europhysics Conference on high energy physics, Marseilles, France, July 1993, Ed. by J. Carr and M. Perrottet, Ed. Frontieres, Gif-sur-Yvettes, 1994.*
S.J.Alvsvaag et al., Proceedings of *The 5th International Conference on Calorimetry BNL, New-York, USA, September 1994.*
S.J.Alvsvaag et al., Proceedings of *The Beijing Calorimetry Symposium, Beijing, China, October 1994, Ed. by H. S. Chen, IHEP, Beijing, 1995.*

[8] T.Camporesi et al., CERN-LEPC 94-13; CERN LEPC 94-16.

[9] M. Bigi et al., "*Luminosity Measurement in 1994 with the STIC detector*", DELPHI note 97-08 PHYS 667

[10] M.Bonesini, M.Paganoni, F.Terranova, S.Gumenyuk, L.Petrovykh, *"The use of artificial neural network for dead channel data recovery in the DELPHI STIC calorimeter"*, DELPHI note 95-169 CAL 129

[11] L.Lönnblad, C.Peterson and T.Rögnvaldsson, *"JETNET 3.0 - A Versatile Artificial Neural Network Package"*, Lund Preprint LU TP 93-29 (1993).

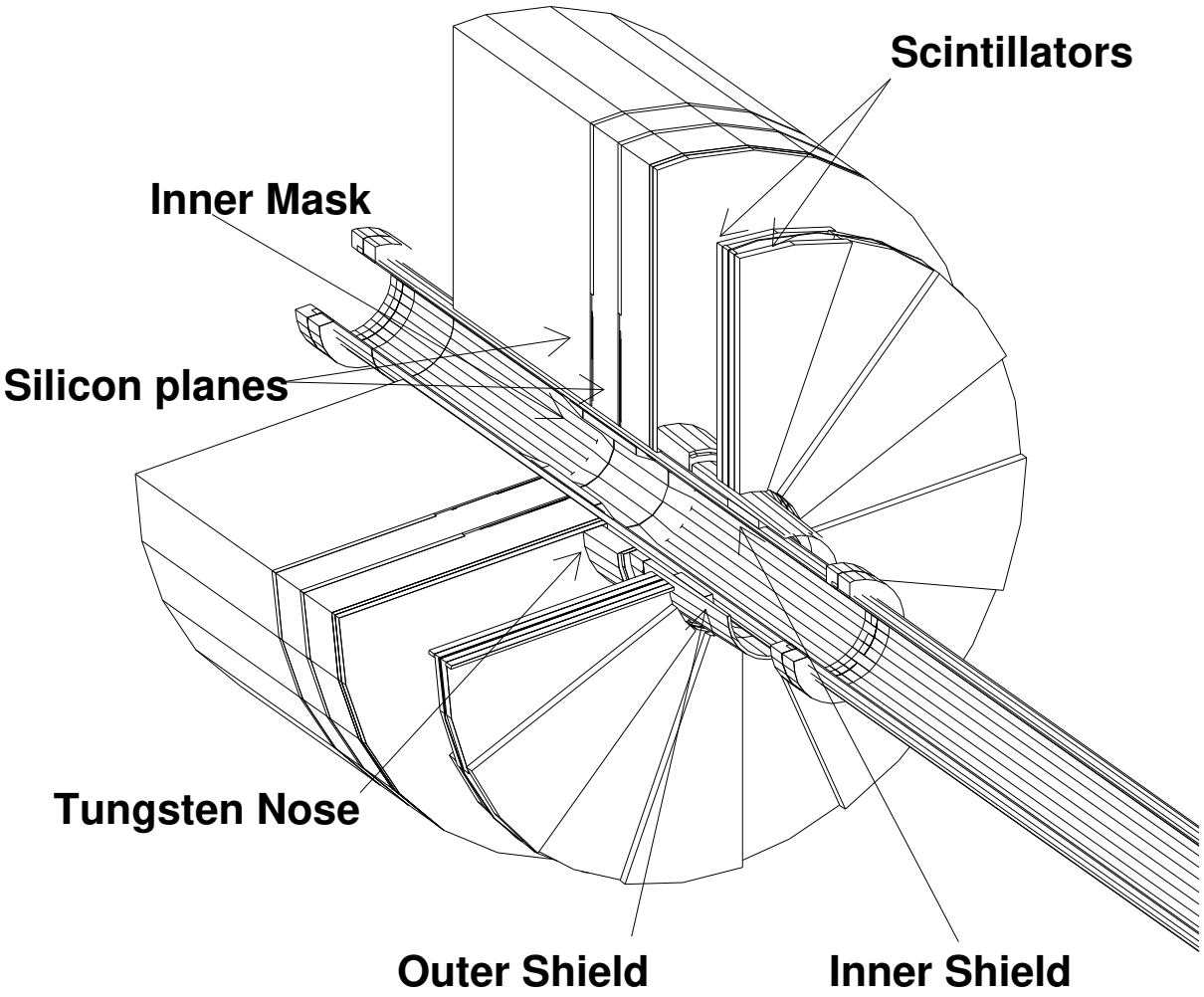

Figure 1: cd /u/xx/stuc/cd /u/xx/stic/prodo View of one arm of the STIC calorimeter

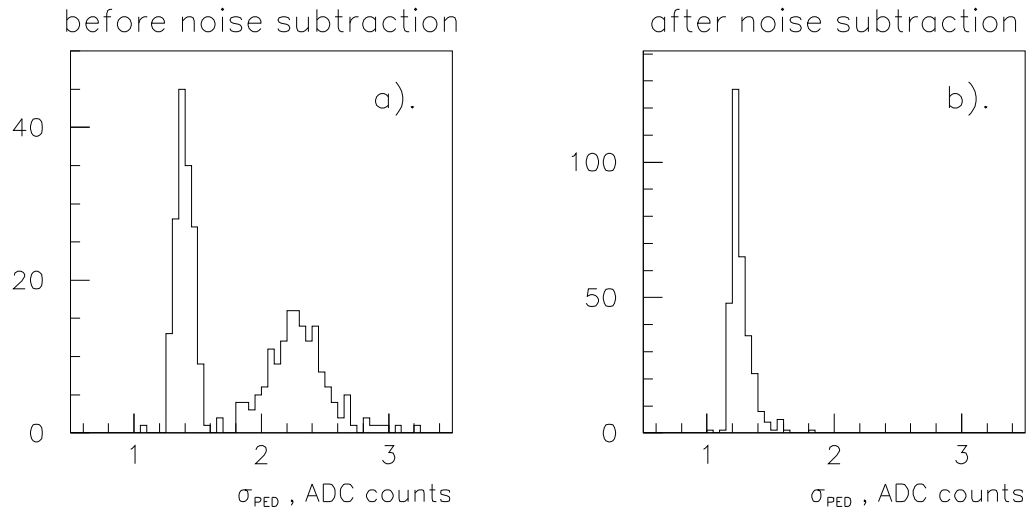

Figure 2: Distribution of the pedestal widths before (a) and after (b) the procedure of common noise subtraction.

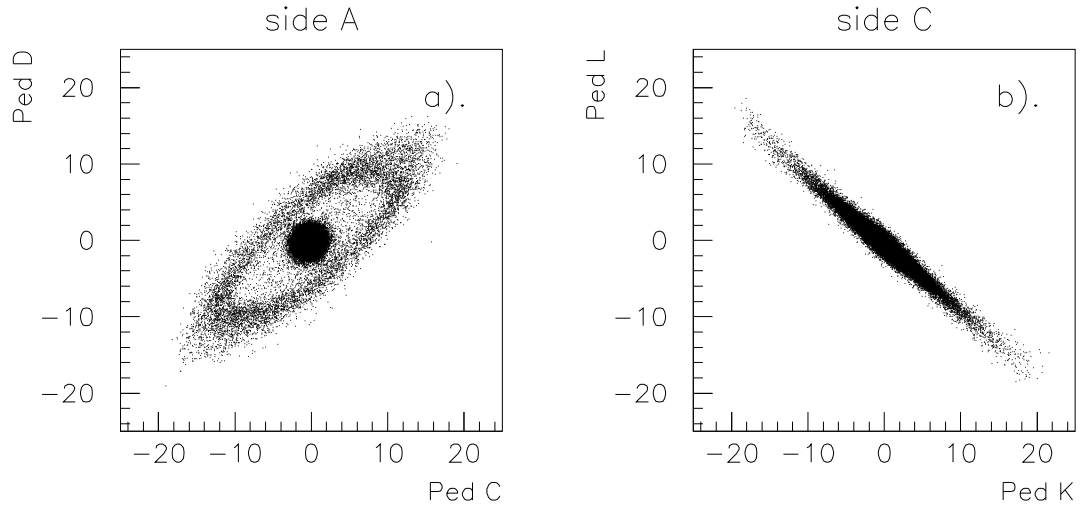

Figure 3: Noise correlation between calorimeter modules during the 1994 data taking (modules C,D are on the A side; modules K,L are on the C side)

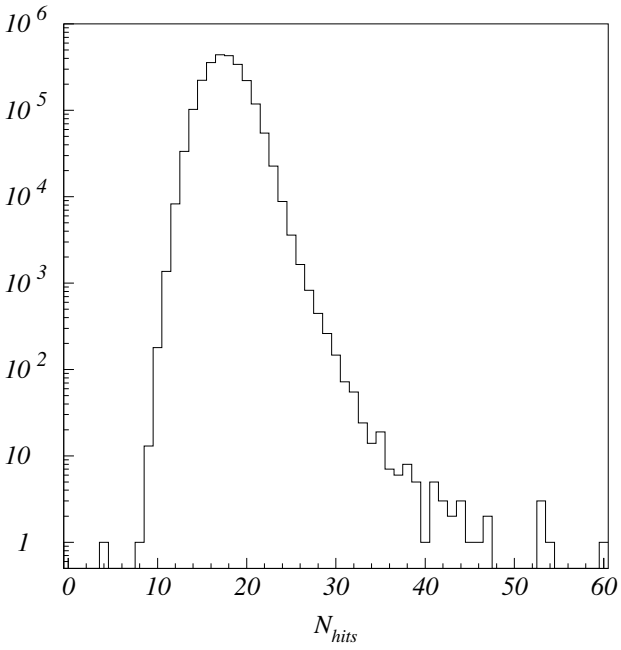

Figure 4: The number of towers belonging to the most energetic cluster, in Bhabha scattering events.

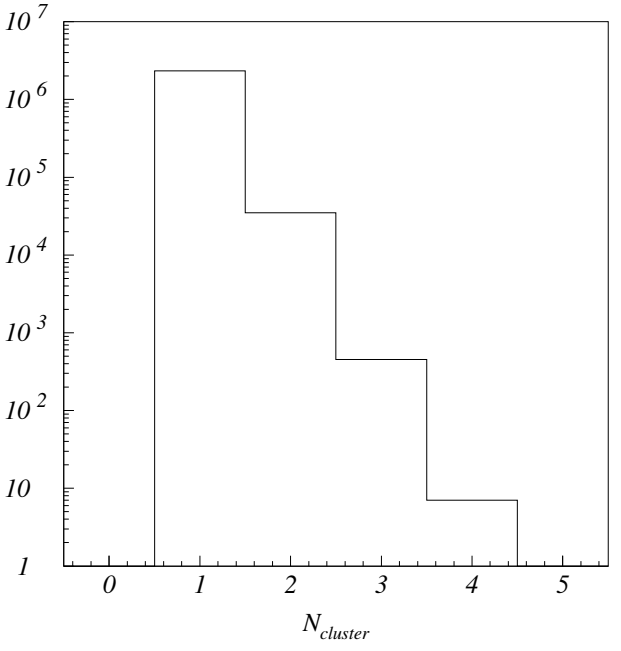

Figure 5: The number of showers reconstructed in one STIC arm, in Bhabha scattering events.

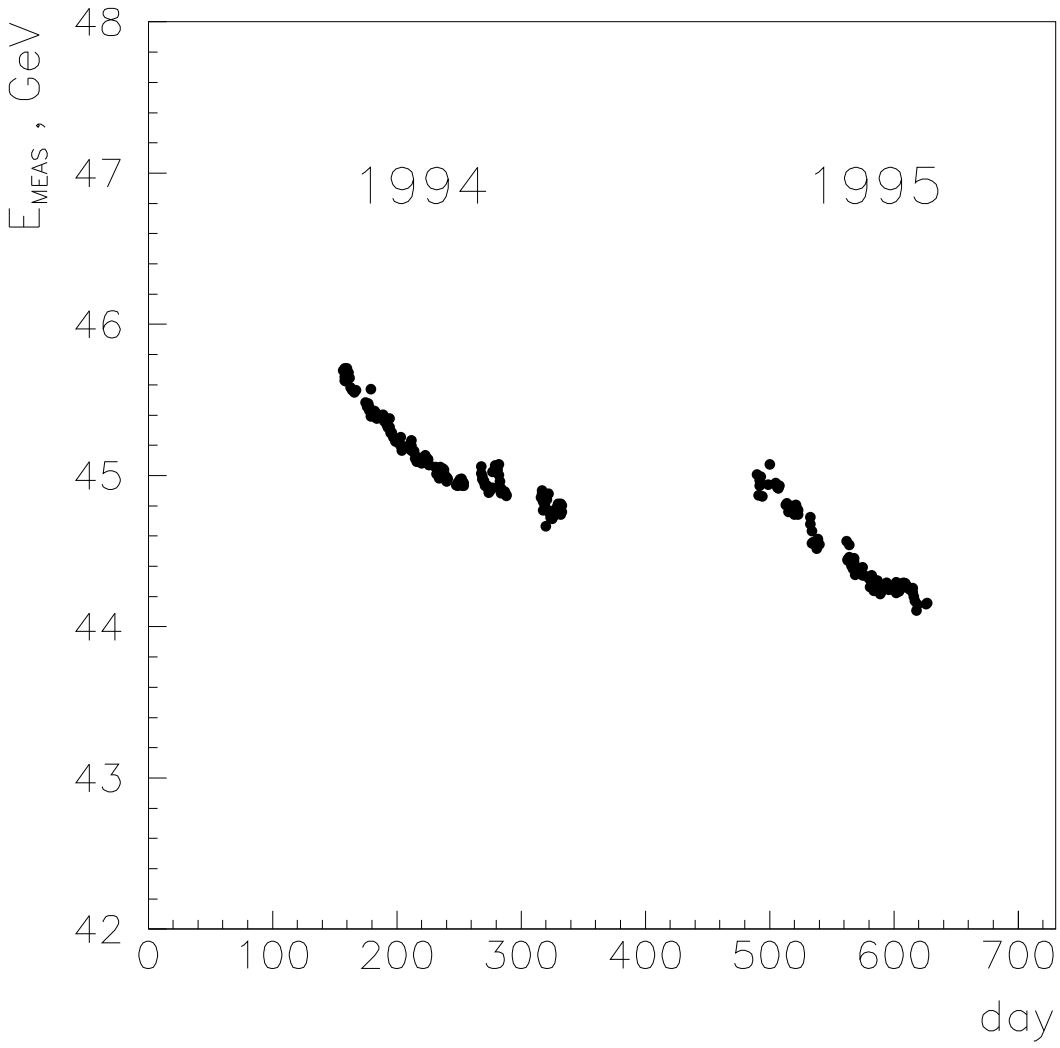

Figure 6: The energy response of STIC to 45 GeV Bhabha electrons versus time, assuming constant calibration coefficients for the 2 years of data taking

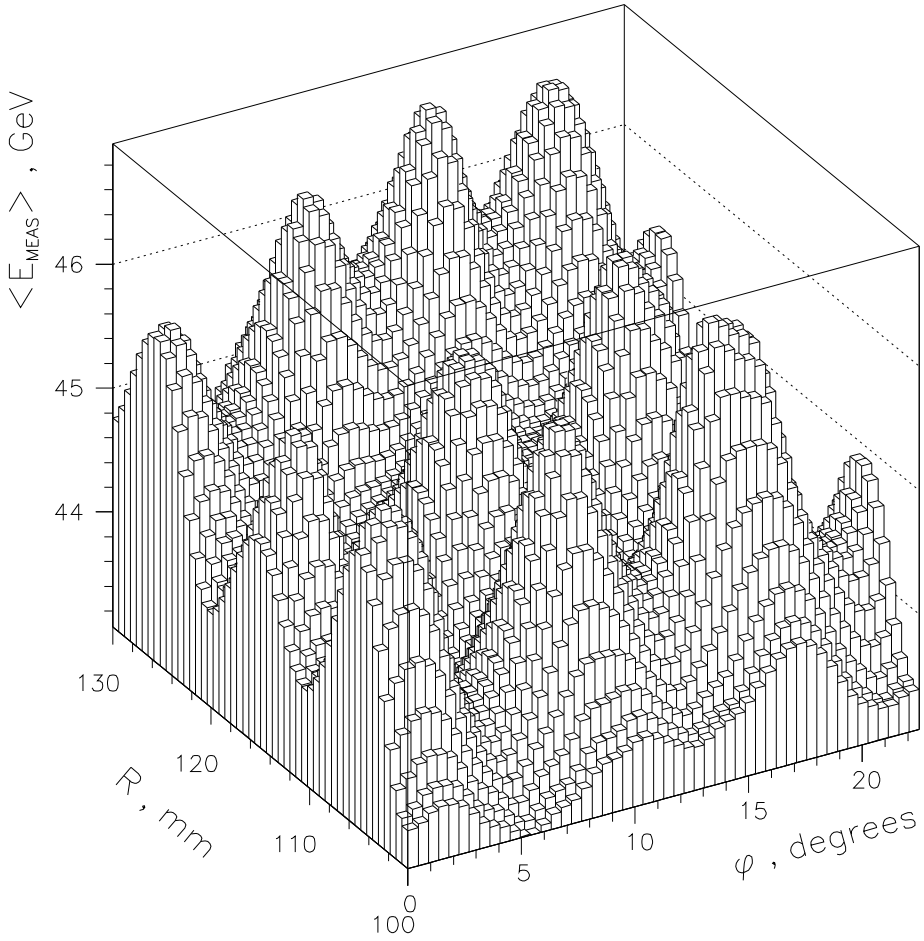

Figure 7: The energy response of STIC to 45 GeV Bhabha electrons versus the impact point in one tower.

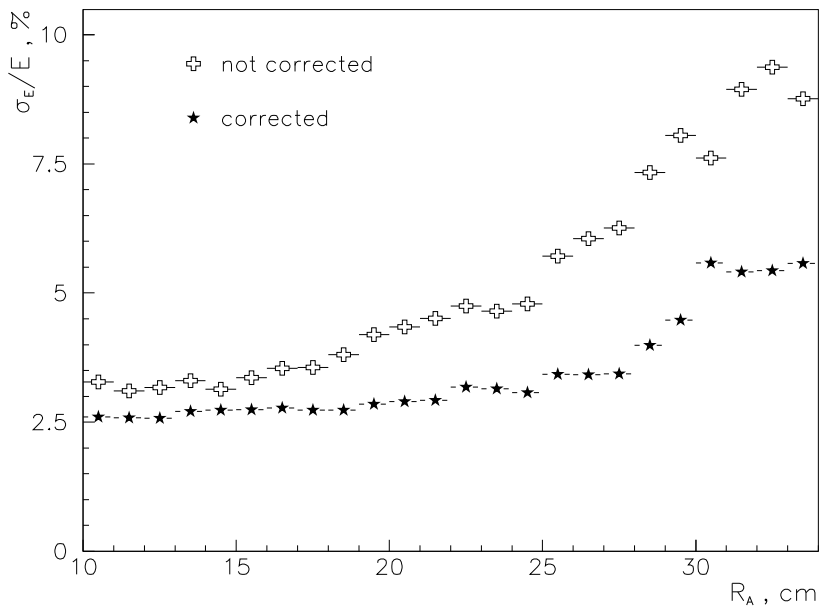

Figure 8: The energy resolution versus radius (side A) before and after correction, for Bhabhas at LEP I .

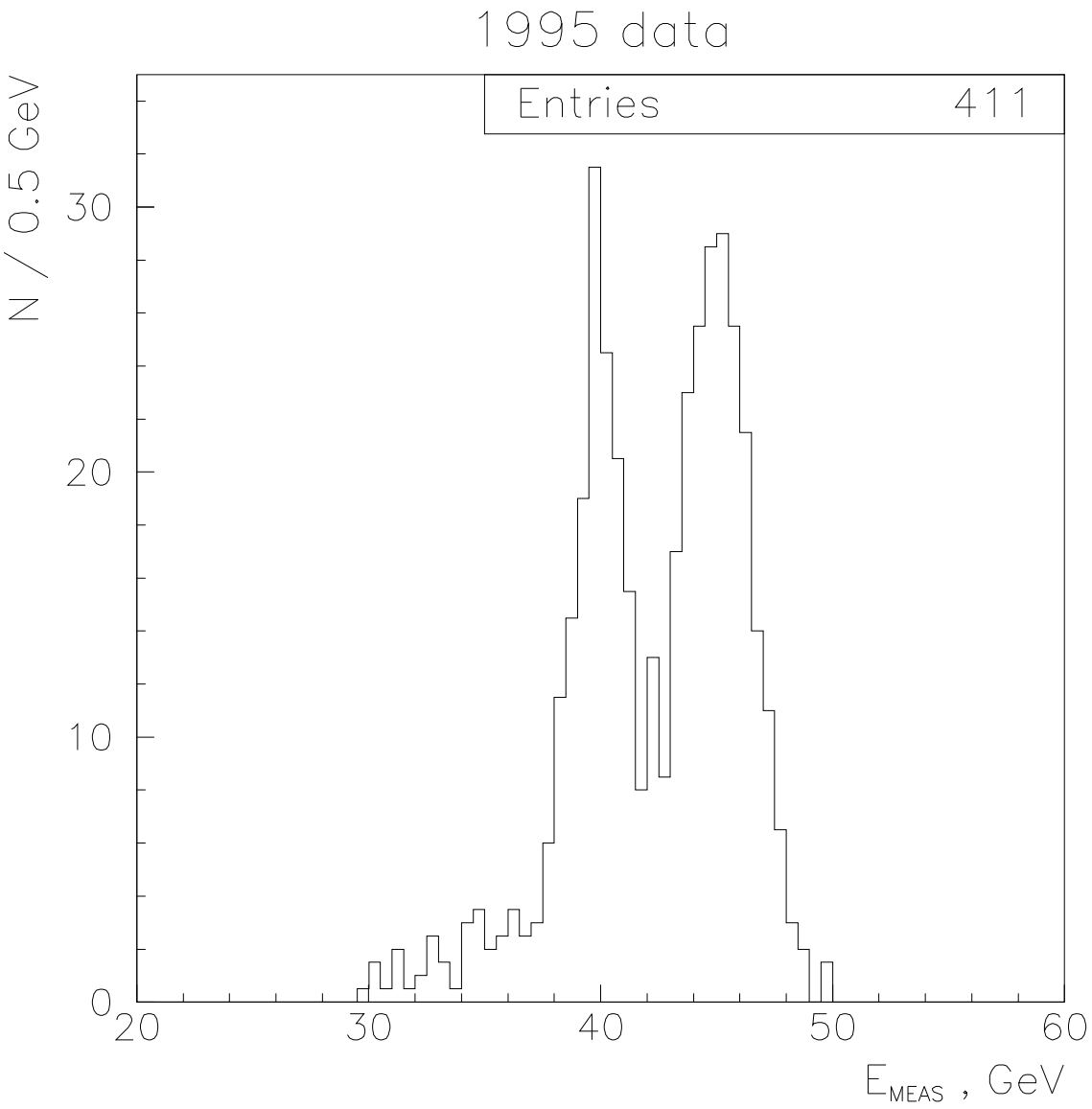

Figure 9: The measured energy spectrum for Bhabha events without wagon tag (411 events out of 1.6 $\times 10^6$).

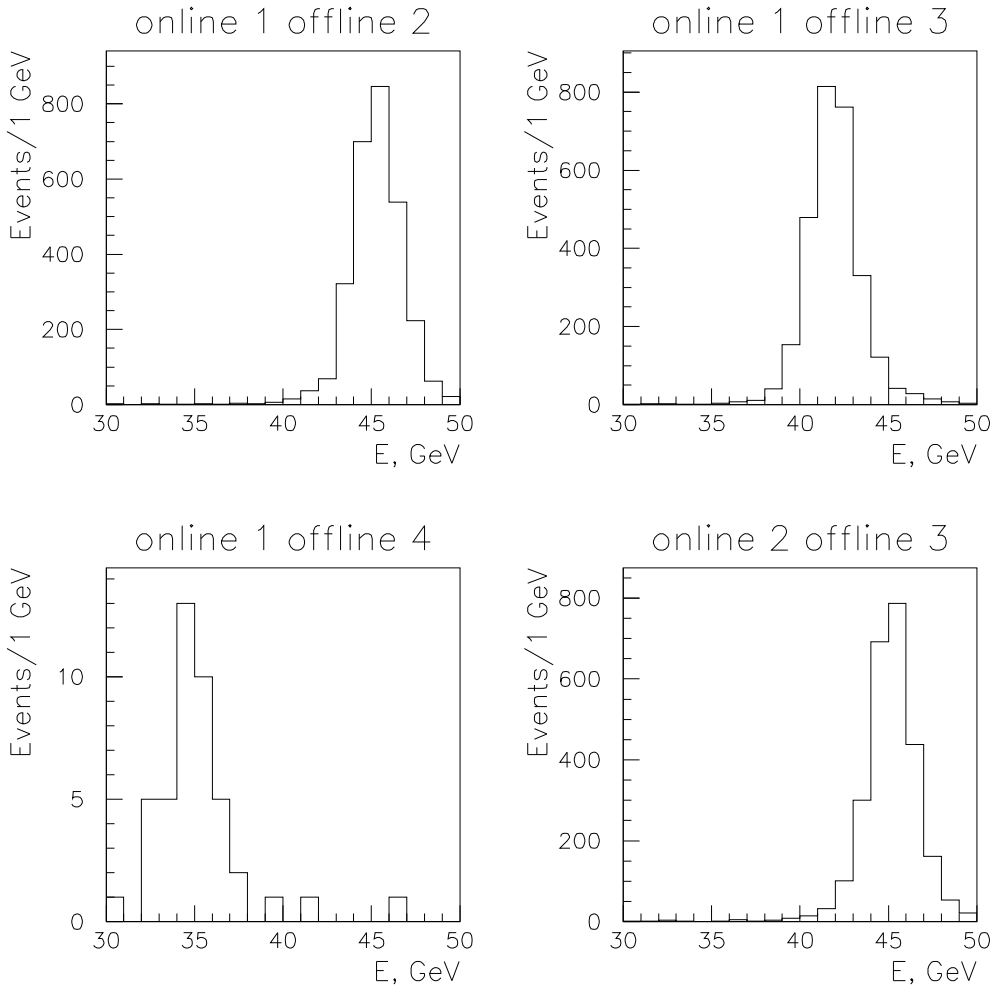

Figure 10: The measured energy spectrum of 45 GeV Bhabha electrons, for various combinations of online and offline wagon tags (in case of ambiguous tag assignement).

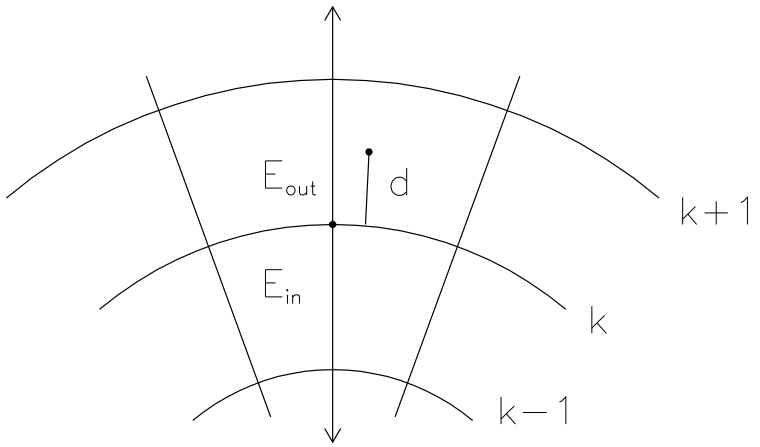

Figure 11: Definition of E_{in} and E_{out} for the measurement of R.

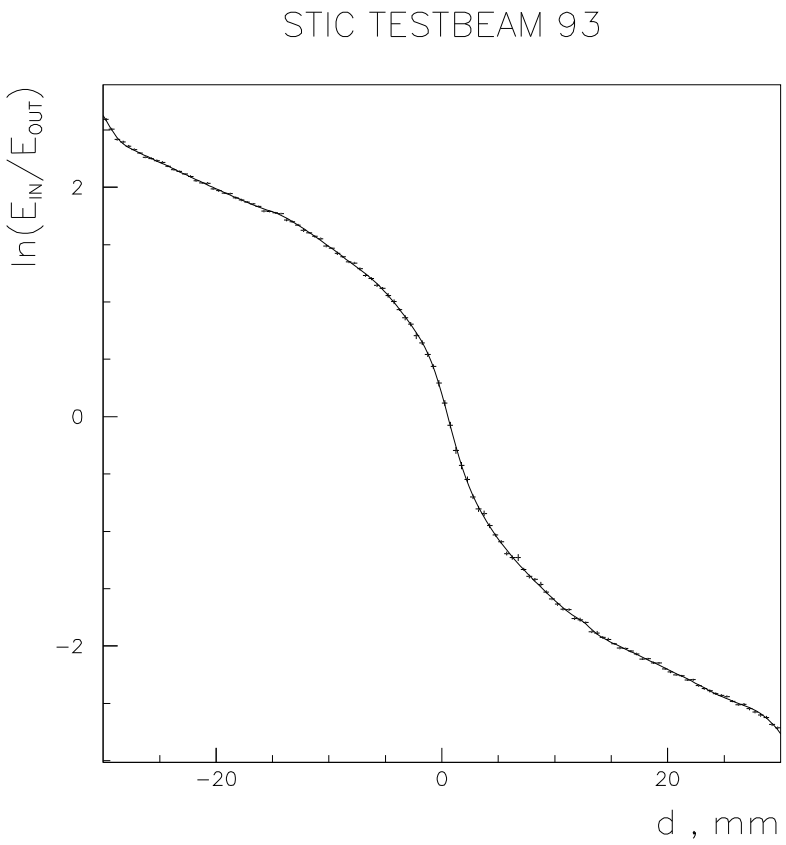

Figure 12: The value of the radial estimator ($\epsilon(d)$) versus the distance (d) from the border between rings 3 and 4, where d was measured by a microstrip telescope in a testbeam.

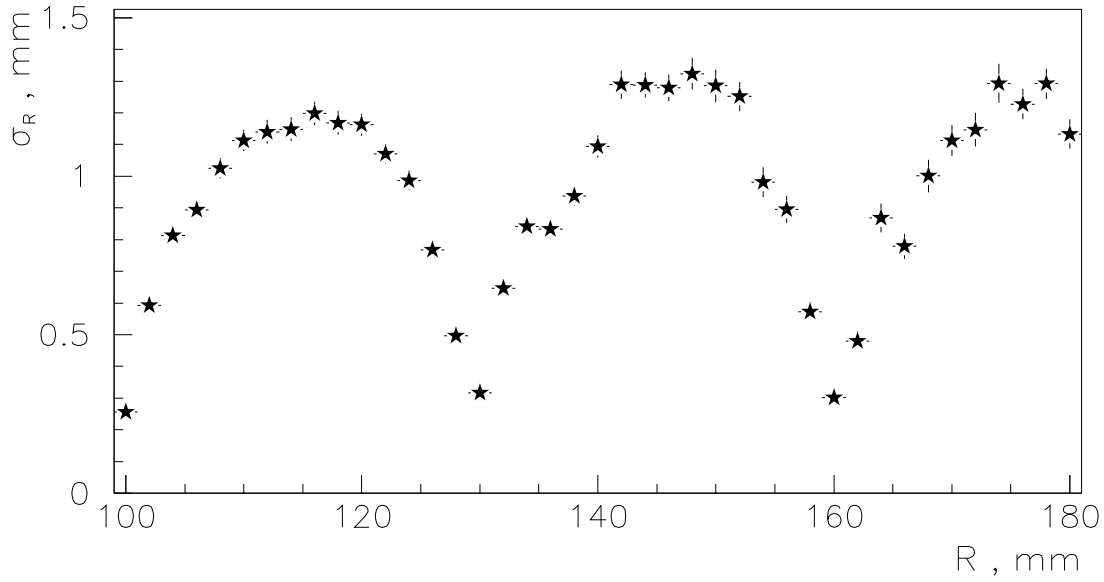

Figure 13: The radial resolution of the calorimeter versus the radius.

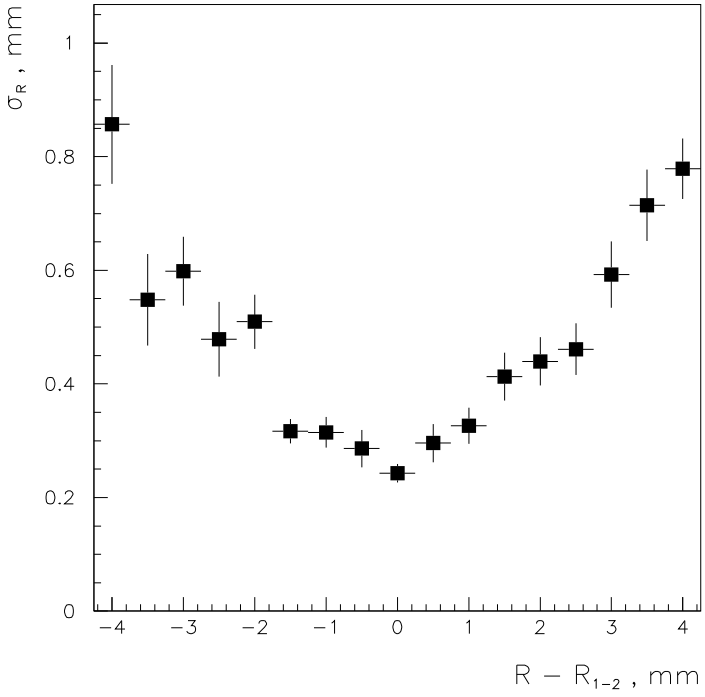

Figure 14: The radial resolution of the calorimeter in the region near to a border between rings.

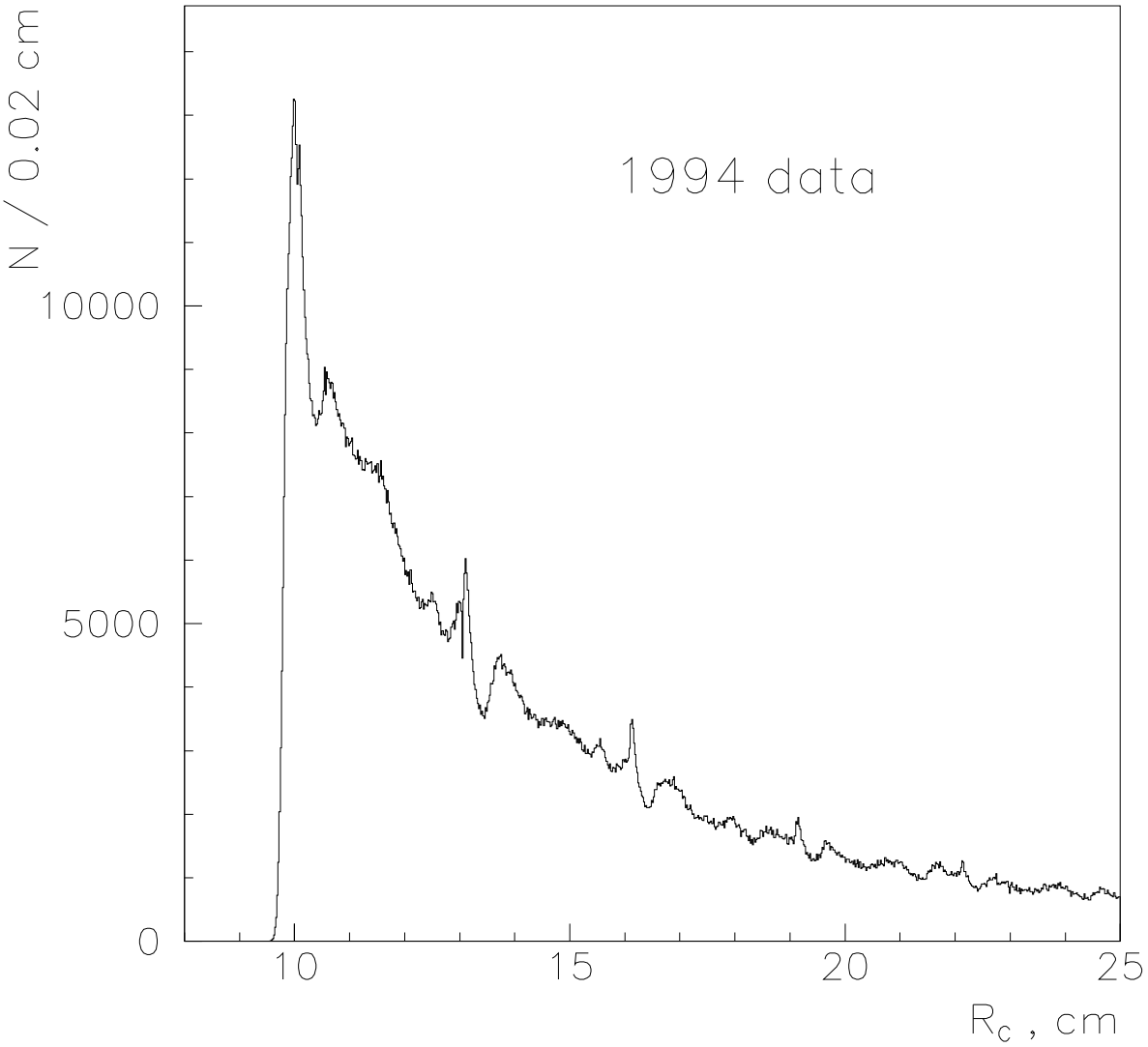

Figure 15: The measured radial distribution for Bhabha events, before corrections.

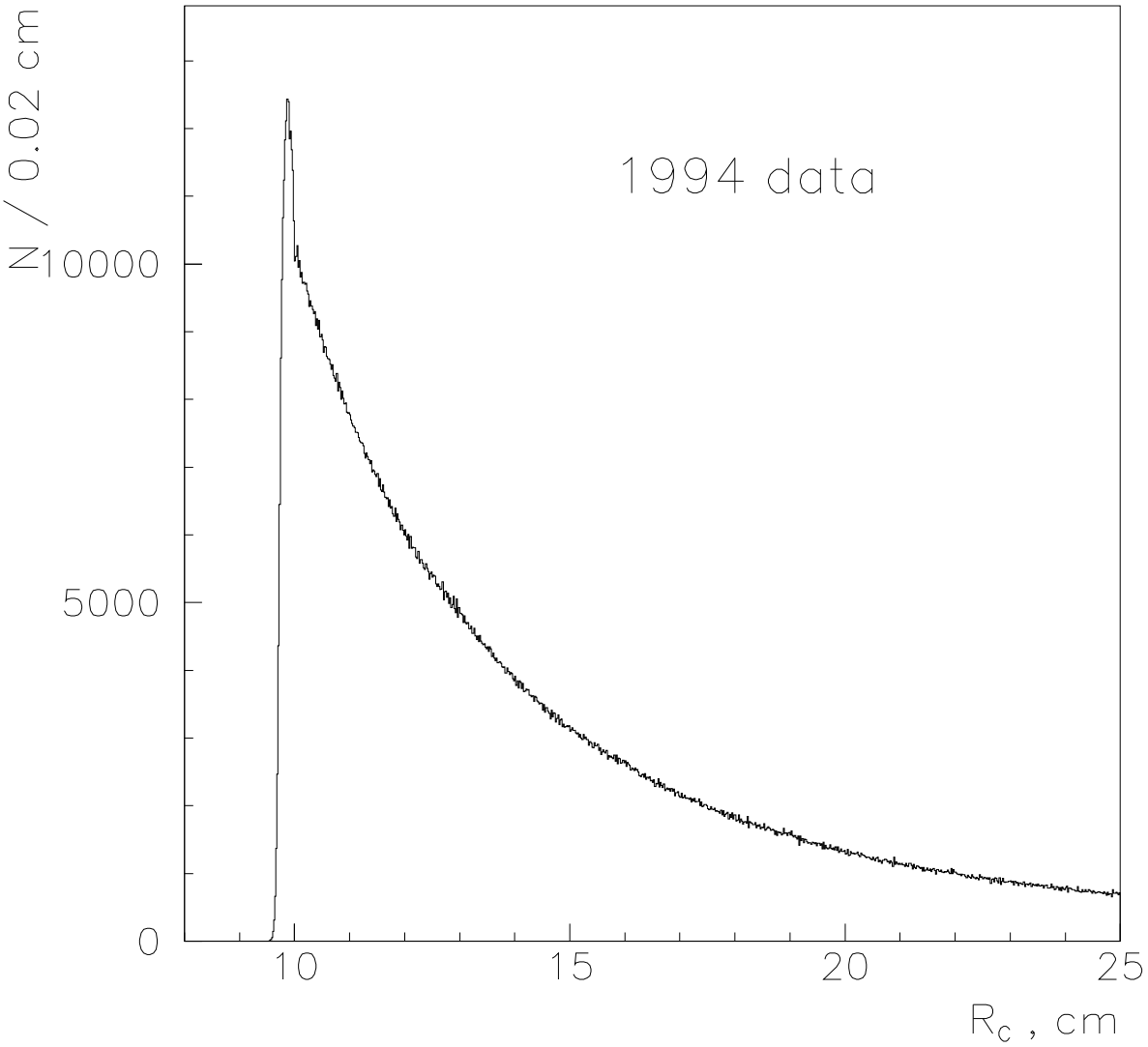

Figure 16: The measured radial distribution for Bhabha events, after corrections.

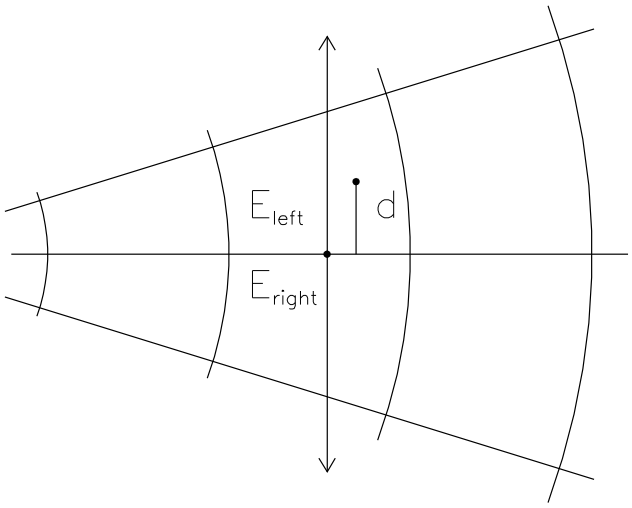

Figure 17: Definition of E_{left} and E_{right} for the estimation of ϕ.

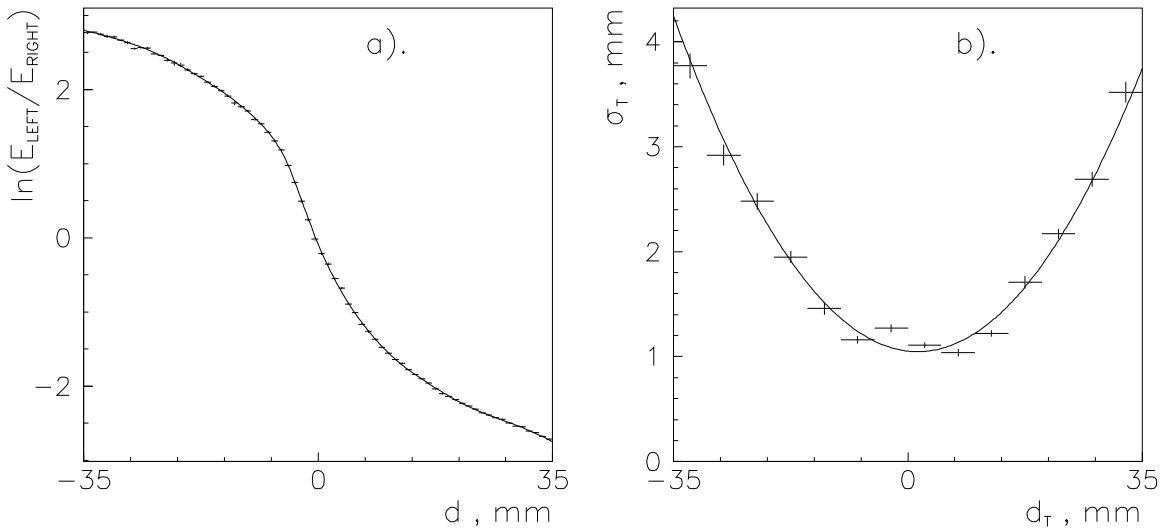

Figure 18: ϕ reconstruction: **(a)** The value of the estimator as a function of the distance to the border between two ϕ-sectors; **(b)** the resolution in the transverse direction versus the distance to the border between two ϕ-sectors.